Modelling the HPRT mutation induction of particle beams: systematic in vitro data collection, analysis and MKM implementation.

Andrea Attili[1], Emanuele Scifoni[2,3], Francesco Tommasino[3,2]

[1] Roma Tre Section, INFN National Institute for Nuclear Physics, 00146 Roma, Italy

[2] Trento Institute for Fundamental Physics and Applications (TIFPA), INFN National Institute for Nuclear Physics, 38123 Trento, Italy

[3] Department of Physics, University of Trento, 38123 Trento, Italy

Corresponding Author:

Andrea Attili

Roma Tre Section, INFN National Institute for Nuclear Physics

andrea.attili@roma3.infn.it

Running title:

MKM modelling of mutation induction for particle beams.

Abstract

Purpose: Since the early years, particle therapy treatments have been associated with concerns for late toxicities, especially secondary cancer risk (SCR). Nowadays, this concern is mainly related to patients for whom long-term survival is expected (e.g. breast cancer, lymphoma, paediatrics). We present a dedicated statistical and modelling analysis aiming at improving our understanding of the RBE for mutation induction ($RBE_{\tilde{M}}$) for different particle species.

Methods: We built a new database based on a large collection of RBE data for mutation induction (i.e. *hprt* mutation assay) from literature (115 entries, distributed among 3 cell lines and 16 particle species). The data were employed to perform statistical and modelling analysis. For the latter, we adapted the microdosimetric kinetic model (MKM) to describe the mutagenesis in analogy to the lethal lesion induction.

Results: When considering all data available, correlation analysis between RBE for survival (RBE_S) and $RBE_{\tilde{M}}$ reveals significant correlation between these two quantities ($\rho=0.86$, $p<0.05$). The correlation gets even stronger when looking at subsets of data based on e.g. cell line, particle species. We also show that the MKM can be successfully employed to describe $RBE_{\tilde{M}}$, obtaining at the same time comparably good agreement with the experimental data and realistic model parameters. Remarkably, in order to improve the agreement with experimental data the MKM requires, consistently in all the analysed cases, a reduced domain size for the description of mutation induction compared to that adopted for survival.

Conclusions: According to our new database, we were able to show that RBE_S and RBE_M are strongly related quantities. We also showed for the first time that the MKM could be successfully applied to the description of mutation induction, representing an endpoint different from the more traditional cell killing. In analogy to the RBE_S, $RBE_{\widetilde{M}}$ can be implemented into TPS evaluations. This might contribute in the future to a more accurate estimation and minimization of secondary cancer risk in particle therapy treatments.

Introduction

Charged particle therapy (CPT) represents nowadays a therapeutic alternative to conventional photon radiotherapy for specific types of cancers and disease sites (Durante *et al* 2021). This goes together with the gradual worldwide spread of CPT centres, the large majority of which is dedicated to proton therapy (Rackwitz and Debus 2019, Durante and Flanz 2019). In parallel to the accumulation of clinical experience and to technological improvements, the spectrum of cancer diseases treated with particles is steadily enlarging. Next to the historical brain and head and neck cancers, protons are currently also considered for e.g. breast cancer, prostate and lymphoma treatments, with clinical trials already on-going. Together with paediatric patients, this raises specific concerns regarding the risk of late radiation effects for patients having a good survival probability and long-life expectancy.

Moreover, the recent introduction in the clinics of different particle types, beside the already established carbon, like e.g. the use of helium at HIT (Krämer *et al* 2016) and the perspective of employing oxygen (Sokol *et al* 2017) and other high LET particles (Mohamad *et al* 2018, Tommasino *et al* 2015) or their combination (Ebner *et al* 2021), forces to include in a cost-benefit analysis also the consideration of such effects for the unconventional radiation fields arising from these particles.

Secondary cancer risk (SCR) resulting from charged particle treatments has been long debated in the past (Paganetti 2012, Balcer-Kubiczek and Eley 2018). Despite that, no clear picture emerged so far allowing a quantitative estimation of SCR in this context.

Obviously, a clinical study in this direction is still hindered by the lack of robust epidemiological data obtained from long-term CPT survivors.

In order to optimize CPT treatments, extensive efforts have been performed to obtain consistent estimation of relative biological effectiveness (RBE, i.e. the ratio of photon to charged particle dose that is needed to observe the same effect) of charged particles for clonogenic cell survival (Friedrich *et al* 2013). These studies, largely based on *in vitro* data, were needed to characterize tumour response and, to a minor extent, normal tissue toxicity. Interestingly, less attention was dedicated to the parameterization of SCR-related endpoints, as for instance mutation induction or cell transformation. Clinical researchers' attention was mainly dedicated to the characterization of the radiation field, in order to estimate the neutron dose contribution arising from nuclear interactions. At the same time, radiation-induced carcinogenesis is a multi-step process, intrinsically more difficult to be captured by cellular experiments compared to cell survival. SCR-related endpoints were investigated in dedicated experimental studies, but attempts to draw a systematic picture have been lacking for a long time. Recently, Hufnagl et al (Hufnagl *et al* 2021) presented a modelling study, based on the Local Effect Model IV (LEM (Scholz *et al* 1997, Friedrich *et al* 2012)), dedicated to the analysis of *in vitro* cell transformation and *in vivo* tumour induction data after charged particle irradiation obtained from literature. Such work presents an attempt to explain experimental observation with a consistent modelling framework, which allows deriving RBE values for cell transformations, in addition to cell survival RBE.

The present work starts with introducing a large and systematic collection of literature data for *in vitro* mutation induction (i.e. *hprt* assay) experiments with monoenergetic particle beams. First, a statistical analysis is performed, and the correlation among survival and mutation parameters is explored in detail. Then, a dedicated modelling analysis is developed and presented, which is based on a specific application of the microdosimetric kinetic model (MKM), which for the first time has been extended to consider simultaneously both survival and mutation endpoints. For the latter, RBE is derived for a broad range of particle species and energies.

Methods

Data Collection

The database presented in this study was obtained by retrieving from literature a large set of available data from *in vitro* mutation induction experiments with charged particles. Such experiments were performed with the *hprt* mutation assay in the time interval 1977-2002. Only publications presenting RBE data for both survival and mutation induction were included (Cox *et al* 1977, 1979, Hei *et al* 1988, Kiefer *et al* 1999, Belli *et al* 1998, Kiefer *et al* 2001, Tsuboi *et al* 1992, Chen *et al* 1994, Cherubini *et al* 2002, Suzuki *et al* 1996, Thacker *et al* 1979, Kranert *et al* 1990, Stoll *et al* 1995, 1996). The assay is based on the selection of cells that after irradiation carry a mutated *hprt* gene, which is present on a single copy on the X chromosome. Mutated cells are selected by the use of a toxic analogue that suppresses not mutated cells; *hprt* mutants finally give rise to colonies. Further details can be found elsewhere (Johnson 2012), while limitations related to the

use of this specific endpoint will be addressed in the Discussion. The database contains 115 entries, distributed among 3 cell lines and 16 particle species. Concerning cell lines, a large prevalence of V79 data is observed. Available data sources are summarized in Table 1, while the full database has been shared online (https://doi.org/10.5281/zenodo.6451956). Specifically, in the shared table a specific ID is assigned to each data entry (i.e. each experimental RBE data), together with information on the cell line and experimental energies/LET. For each entry, Linear-quadratic (LQ) parameters α and β values are also reported for survival and mutation induction endpoints both as retrieved from the original publication (when available) and as obtained by performing a LQ fit on raw data for survival and mutation induction. The raw dose-response data were collected by manually digitalizing the survival/mutation curves, when available. Importantly, the accuracy of the digitalization process was limited in some cases by the poor quality of the original figures, especially for the oldest publications. In some cases, this might also have an impact on the quality of LQ fit.

Table 1. Schematic overview of the data collection performed for the present study.

Cell Line	Nr. of entries	Particle Species	References
V79*	83	H, He, B, C, N, O, Ne, Ca, Ti, Ni, Xe, Au, Pb, U	Cox77, Thacker79, Kranert90, Stoll95, Stoll96, Belli98, Kiefer99, Kiefer01, Cherubini2002, Govorun2002
HF19/HSF*	24	H, He, B, N, Ne, Ar, Fe, La	Cox77, Cox79, Hei88, Tsuboi92, Chen94
HE*	8	C	Suzuki96

* V79 are Chinese hamster cells, HF19/HSF are human fibroblasts, HE are human embryo cells

Statistical analysis

Linear correlation between RBE for survival (RBE_S) and mutation induction ($RBE_{\tilde{M}}$) was investigated by evaluating the Pearson correlation coefficient, together with the corresponding p-values. Data for each particle species were analysed separately, as well as correlation was calculated by pooling together all available data. Unless specified, in this work RBE for both endpoints always refers to RBE_α, which is the asymptotic RBE obtained by the ratio of ion and photon α parameters and indicates the maximum achievable RBE (i.e. RBE_α or RBE for $D \rightarrow 0$).

Mutation induction Modelling

The modelling framework is based on the use of the MKM version according to the Monte Carlo time dependent approach introduced by Manganaro et al. (Manganaro *et al* 2017), in a context inspired by the recent publication by Hufnagl et al. (Hufnagl *et al*

2021). Considering the significant correlation observed between RBE_S and RBE_M, the basic idea for modelling mutation induction is to use the MKM kinetic equations to describe the induction and repair of lesions that result in both survival and mutation endpoints. In the case of survival, the kinetic equations are written as (Hawkins 1998) :

$$\begin{cases} \dot{x}_{cd} = \lambda \dot{z}_{cd} + a y_{cd} + b(y_{cd})^2 \\ \dot{y}_{cd} = k\dot{z}_{cd} - (a+r)y_{cd} - 2b(y_{cd})^2 \cong k\dot{z}_{cd} - (a+r)y_{cd} \end{cases} \quad (1)$$

Where x and y are, respectively, irreparable and repairable lesions, while z indicates the microscopic (specific) absorbed dose. The indexes c and d refer to the specific cell and domain considered, respectively. The rate of production of irreparable ($\dot{x}$) and repairable ($\dot{y}$) lesions is proportional to the dose rate ($\dot{z}$), with proportionality constants λ and κ, respectively. Irreparable lesions are associated with clustered DNA damages which are directly lethal for the cell, while repairable lesions identify with lethal damage that can be repaired with constant rate r, spontaneously converted to irreparable damages with first-order constant rate a or undergo pairwise combination with another reparable damage and be promoted to an irreparable lesion in a second-order process with constant rate b. In the case of ion irradiation the quadratic $2b(y_{cd})^2$ term in Eq. (1) is usually neglected when compared with first-order terms (Hawkins 1996, Inaniwa *et al* 2013, Inaniwa and Kanematsu 2018).

When considering mutation induction, which stems from a similar concept of DNA lesions' evolution dynamics, the kinetic equations can be considered to follow a similar conceptual framework, and can be written as:

$$\begin{cases} \dot{x}'_{cd'} = \lambda' \dot{z}'_{cd'} + a' y'_{cd'} + b' (y'_{cd'})^2 \\ \dot{y}'_{cd'} = k' \dot{z}'_{cd'} - (a' + r') y'_{cd'} \end{cases} \quad (2)$$

Where the parameters a', b' and r' describe the production and repairing rates of lesions related to the mutation endpoint. These parameters are in principle numerically different from the ones used in the survival Eq. (1). Furthermore, also the domain index and the corresponding specific energy could change, namely $d' \neq d$ and $z'_{cd'} \neq z_{cd}$, since, in principle, the relevant domain sizes could differ for the two endpoints.

Assuming a Poisson distribution probability for the number of irreparable lesions on a cell for both survival and mutation, the surviving probability S for the irradiated cell population can be calculated as:

$$S = \langle S_c \rangle_c = \langle exp\ (-\sum_{d=1}^{N_d} x_{cd}(t)) \rangle_c = \frac{1}{N_c} \sum_{c=1}^{N_c} exp\ (-\sum_{d=1}^{N_d} x_{cd}(t)), \quad (3)$$

where S_c is the expected survival for the cell c, while the probability to have no mutation μ is:

$$\mu = \langle \mu_c \rangle_c = \langle exp\ (-\sum_{d'=1}^{N'_d} x'_{cd'}(t)) \rangle_c = \frac{1}{N_c} \sum_{c=1}^{N_c} exp\ (-\sum_{d'=1}^{N'_d} x'_{cd'}(t)), \quad (4)$$

where μ_c is the expected no-mutation outcome for the cell c. The number of lesions x_{cd} and $x'_{cd'}$ are the solutions of Eq. (1) and (2) and the average is performed over a cell population large enough to achieve statistical convergence. Solving explicitly for $t \to \infty$ we can extract a linear-quadratic behaviour for both survival (Eq. (3)) and mutation (Eq. (4)) (see for details (Manganaro *et al* 2017)):

$$S = \langle \exp\ (-\frac{\alpha_0}{N_d} \sum_{d=1}^{N_d} z_{cd} - \frac{\beta_0}{N_d} \sum_{d=1}^{N_d} (z_{cd})^2) \rangle_c \quad (5)$$

$$M = \langle \exp\left(-\frac{\alpha'_d}{N'_{d'}}\sum_{d'=1}^{N'_{d'}} z'_{cd'} - \frac{\beta'_0}{N'_{d'}}\sum_{d'=1}^{N'_{d'}}(z'_{cd'})^2\right)\rangle_c \quad (6)$$

In the limit of low LET irradiations, Eq. (5, 6) can be approximated as (Hawkins 1998):

$$S(D) \sim exp\left(-(\alpha_0 + \beta_0 \underline{z}_{1d})D - \beta_0 D^2\right) \quad (7)$$

$$\mu(D) \sim exp\left(-(\alpha'_0 + \beta'_0 \underline{z}'_{1d'})D - \beta'_0 D^2\right) \quad (8)$$

where D is the macroscopic dose and $\underline{z}_{1d}$ and $\underline{z}'_{1d'}$ indicate the dose-mean specific energies evaluated in the respective domains.

The evaluation of the specific energy distributions is performed using an amorphous track model based on the Kiefer-Chatterjee track model introduced in (Kase *et al* 2008) while the domains of the cell nucleus have a cylindrical symmetry and are arranged in a close-packed structure (Manganaro *et al* 2017). It should be noted that in our formulation, following the basic concept of dual radiation action (Kellerer and Rossi 1978), the definition of a domain does not stick to a biological substructure, as sometimes intended in the MKM approach; it rather refers, instead, to a physical sampling volume used to identify the proximity of two lesions for the specific effect. We remark that, according to this interpretation, we can expect a domain size that can be in general different according to the specific endpoint considered.

An example of the evaluation of the specific energy spectra obtained from the MC evaluations is reported in Figure 1 in the exemplary cases of irradiation with proton beam for two different domain radii and imposed macroscopic dose $D = 2$ Gy.

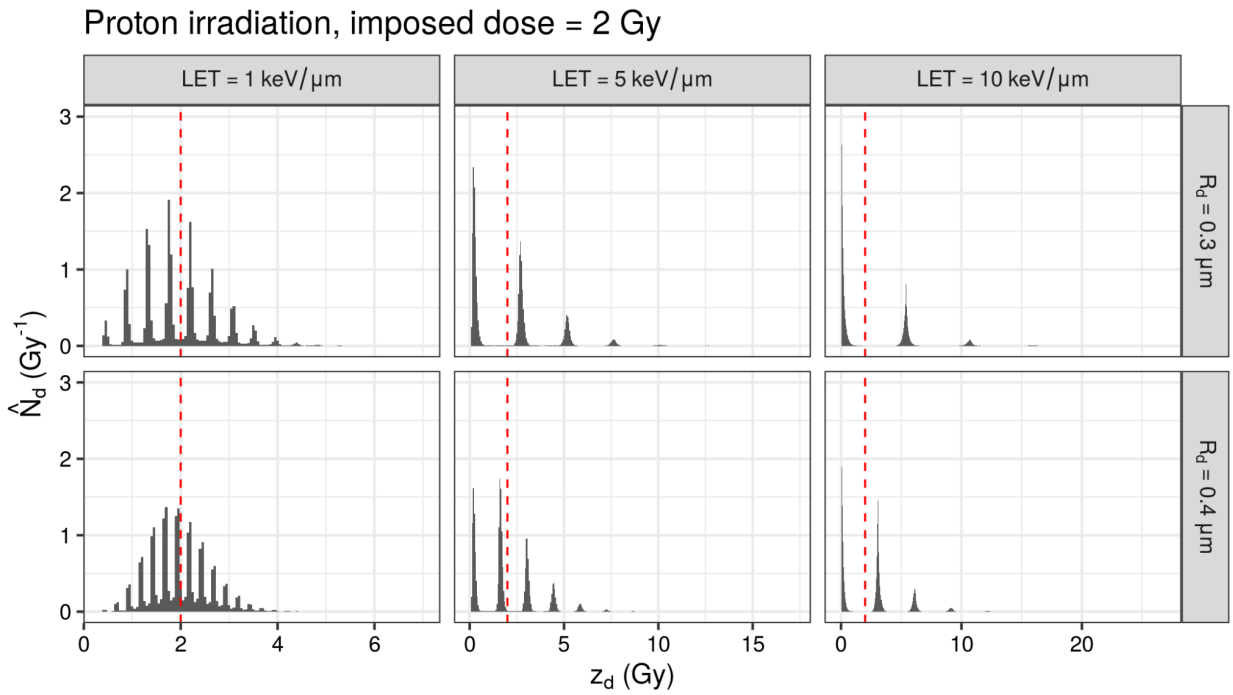

Figure 1: An example of the probability density distribution $\hat{N}_d(z_d)$ for the energy deposited in a domain d. The distribution is evaluated for monoenergetic proton beam irradiations with LET = 1, 5 and 10 keV/µm in water and for two different domain sizes (R_d = 0.3 and 0.4 µm). These sizes represent common values used in literature for MKM evaluations. The macroscopic deposited dose is $\bar{z}_d = D = 2$ Gy (vertical dashed line.) The discrete peaks correspond to the passage of 0, 1, 2, … particles.

By repeating the MC evaluations to evaluate Eq. (5) and (6) for a sequence of different macroscopic imposed doses, it is possible to reproduce the dose response curves for survival and mutation, $S(D)$ and $\mu(D)$. These curves can be fitted with the LQ formulae:

$$S(D) = exp(-\alpha D - \beta D^2) \qquad (9)$$

$$\mu(D) = exp(-\alpha' D - \beta' D^2).$$

In order to describe survival and mutation induction with a consistent approach, few other quantities need to be introduced. First, it is necessary to keep in mind that the dose-response for observable mutations follows a bell-shaped curve, which is the result of two concurrent processes as the dose is enhanced, namely the increase in the number of

induced mutations and the decrease in the number of surviving cells. In other words, while the number of radiation-induced mutations is expected to increase monotonically with dose, we are only able to observe the mutations carried over by surviving cells, i.e., the *surviving mutants* as reported in several experiments, which tend to zero for increasingly high doses. Therefore, we need to distinguish between the probability of visible mutation per surviving cell ($\widetilde{M}$), i.e. the relevant quantity that can be measured in experiments, and the overall probability of induced mutations (M). Here we are using the same notation adopted by Hufnagl et al. (Hufnagl *et al* 2021) for consistency.

Concerning the overall induced mutations, we can now define:

$$M = (1 - \mu) = (1 - \langle \mu_c \rangle_c) \tag{10}$$

Since the survival and mutation probabilities are correlated at the level of the single cell, the probability of observable mutations can be defined as the average of the products of the probabilities:

$$P = \langle S_c(1 - \mu_c) \rangle_c \tag{11}$$

while the probability of visible mutation per survivor can be evaluated as:

$$\widetilde{M} = P/S. \tag{12}$$

Following the LQ formalism in Eq. (9) we can also express the probability of observable mutations per survivor as:

$$\widetilde{M} = 1 - exp\,(-\tilde{\alpha}D - \tilde{\beta}D^2) \tag{13}$$

where, due to the correlation, in general $\tilde{\alpha} \neq \alpha'$ and $\tilde{\beta} \neq \beta'$.

The MC-MKM procedure for the evaluation of the correlated probabilities S, M and $\tilde{M}$ is summarized in Figure 2, showing that the number of lesions' distribution for each simulated cell is evaluated and then averaged to obtain the expected probability of survival and induced mutation for that specific cell. This leads to the dose response curve for observable mutation displayed in the middle panel. Finally, by repeating the procedure for the LET values of interest and by fitting the dose response curves with Eq. (9) and (13), the typical dependence of RBE shown in the right panel as a function of LET is observed for the quantities introduced so far, which are plotted separately.

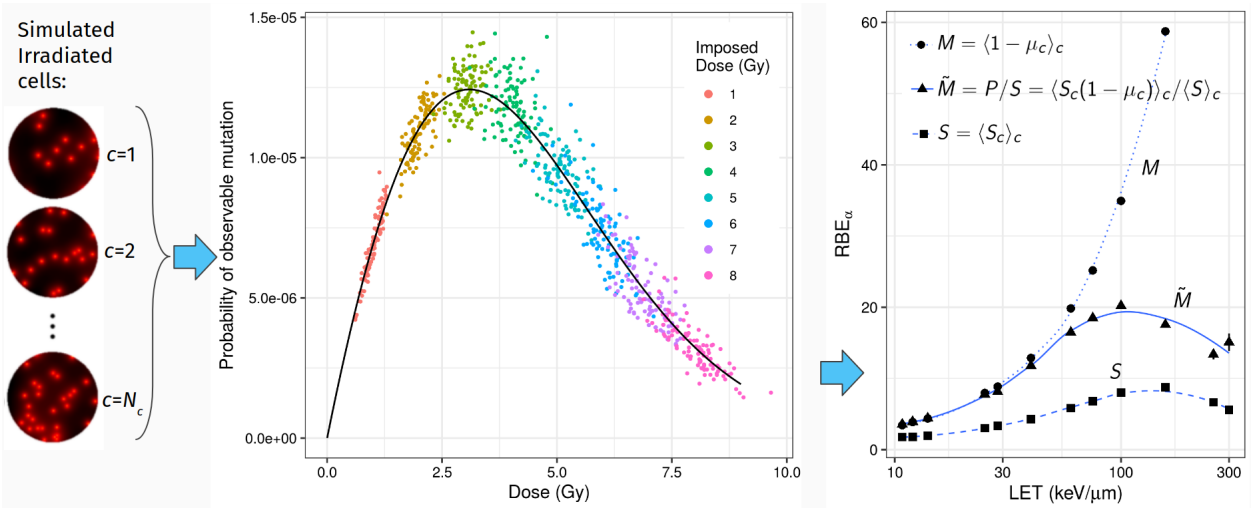

Figure 2: Schematic representation of the present modeling workflow. Monte Carlo simulation provides information on the lesion distribution for individual cells according to the MKM formalism (left). The probability of observable mutations P is then obtained by combining the survival with the mutation induction probability and averaging over the population of simulated cells for different imposed doses (middle). The dots represent the product $(1-\mu_c)S_c$ versus D_c, the dose received by the cell c. The continuous line is the average $P = \langle S_c(1-\mu_c)\rangle_c$ versus $D = \langle D_c\rangle_c$. The procedure can be repeated for any particle/energy of interest, thus allowing to retrieve RBE_α as the ratio of ion to photon LQ parameters both for survival and observable mutations. Representative RBE_α values as a function of LET are shown in the right plot for the endpoints of interest.

Identification of the MKM parameters

Following the idea introduced in (Kase *et al* 2008), since in the case of low-LET gamma-rays irradiation $\underline{z}_{1d}$ and $\underline{z'}_{1d}$, are both negligible, from Eqs. (7) and (8) (α_0, β_0) and (α'_0, β'_0) can be operatively identified as the experimental LQ parameters for the respective endpoints with gamma reference radiation, (α_x, β_x) and (α'_x, β'_x). In the low-LET limit, when homogeneous dose distribution is expected in the cell, the fluctuations of the energy deposition pattern among cells are negligible. As a consequence the correlation between μ_c and S_c is lost and cell survival and mutation can be considered as two independent processes. In this limit, in particular in the case of photon irradiation, one can approximate $\widetilde{M} \simeq M$. Consequently it is possible to identify experimentally the MKM LQ parameters for both mutation and survival by using the corresponding photon experimental data (Hufnagl *et al* 2021):

$$\alpha_0 \simeq \alpha_x, \qquad \beta_0 \simeq \beta_x, \tag{14}$$

$$\alpha'_0 \simeq \alpha'_x \simeq \tilde{\alpha}_x, \qquad \beta'_0 \simeq \beta'_x \simeq \tilde{\beta}_x.$$

In order to apply the MKM formalism Eqs. (14) can be used to fix the radiosensitivity parameters independently. For this purpose, photon α and β values must be available for both survival and mutation. Moreover, the size of the cell nucleus (i.e. the nuclear radius), R_N, as well as the domain sizes, R_d and R'_d, must be defined. For this study, data retrieved from each publication were considered as an independent data set. Since not always reported in the original publication, photon parameters were obtained by performing a linear quadratic fit on the survival and mutation dose response curves, thus

assigning a value to survival (α_0, β_0) and mutation (α'_0, β'_0) parameters. In order to fix the nuclear size, a fit based on the MKM formalism was then performed on the experimental survival RBE data, $RBE_S = RBE_\alpha = \alpha/\alpha_x$, as a function of LET for that specific data set, by keeping fixed $\alpha_0 = \alpha_x$ and $\beta_0 = \beta_x$ and obtaining as output the nuclear radius R_N and the domain size R_d. The same nuclear radius was then adopted also for the mutation analysis, $R'_N = R_N$, in addition to $\alpha'_0 = \alpha'_x$, $\beta'_0 = \beta'_x$, while variations to the domain size R'_d were allowed until a minimum χ^2 was reached.

Limits of applicability and data selection

The modelling analysis was performed on a subset of the available experimental data. Specifically, exclusion criteria were the lack of photon parameters, the use of an endpoint for RBE different from RBE_α, reporting too few data points for a consistent analysis and the use of particles heavier than oxygen being not of interest for clinical applications. Moreover, we restricted the modelling analysis to V79 cells since this cell line is the one where systematic experimental data is available. In the case of human fibroblast, the data is associated to $\beta_0 \cong 0$ for both survival and mutation endpoints. This limits the applicability of the MKM, which requires a $\beta_0 > 0$.

The proposed model relies on the assumption of track segment condition, i.e. a constant stopping power is assumed when the particles cross the cell nucleus (diameter ~ 10 μm). This approximation is reasonable for particles that have kinetic energies not too low and LET not too high, that otherwise should be excluded in the analysis. Furthermore, we verified that in the case of nuclei with $R_d \neq R'_d$, very high LET particles (LET > 300

keV/μm) produce a slight decorrelation effect, that manifests in an overestimation of the correlated probability of observable mutations P. This effect is an artifact that arises in the Monte Carlo evaluation of slightly different geometrical domain structures, when the radial size of the track model is of the order or smaller than the domain sizes used implemented for both mutation and survival. For all these reasons particles with LET > 300 keV/μm have been excluded in the following analysis.

Results

All data points retrieved from literature are collected in Figure 3, where $RBE_{\tilde{M}}$ as a function of LET is shown and data for different particle species are plotted separately. The figure suggests the tendency of an $RBE_{\tilde{M}}$ increasing with LET up to the point when a broadened peak is reached at around 100 keV/μm, before decreasing again at the highest LET values. This trend, which is more evident for V79 due to the larger data abundance, is observed for the four cell lines considered here.

A correlation analysis between RBE_S and $RBE_{\tilde{M}}$ was conducted, which is shown in Figure 4. When pooling together all available data, the figure (left panel) suggests a strong correlation ($\rho=0.86$, $p<0.005$) as well as the tendency of enhanced RBE values for mutation induction compared to survival, especially for particles heavier than protons. Hufnagl et al observed a similar trend in their analysis of cell transformations (Hufnagl *et al* 2021). When looking at the single particle species, the correlation is even stronger for H and He, while it gets gradually lower for increasing particle charge (inserts in Figure 4). Specifically, correlation looses significance for C, O and Ne, but the reduced statistics

might also play a role here. The frequency distributions of RBE_S and $RBE_{\tilde{M}}$ for the different particle species are also reported in the figure at the top and right axis, respectively. This indicates that experimental data are quite scattered and cover large RBE ranges.

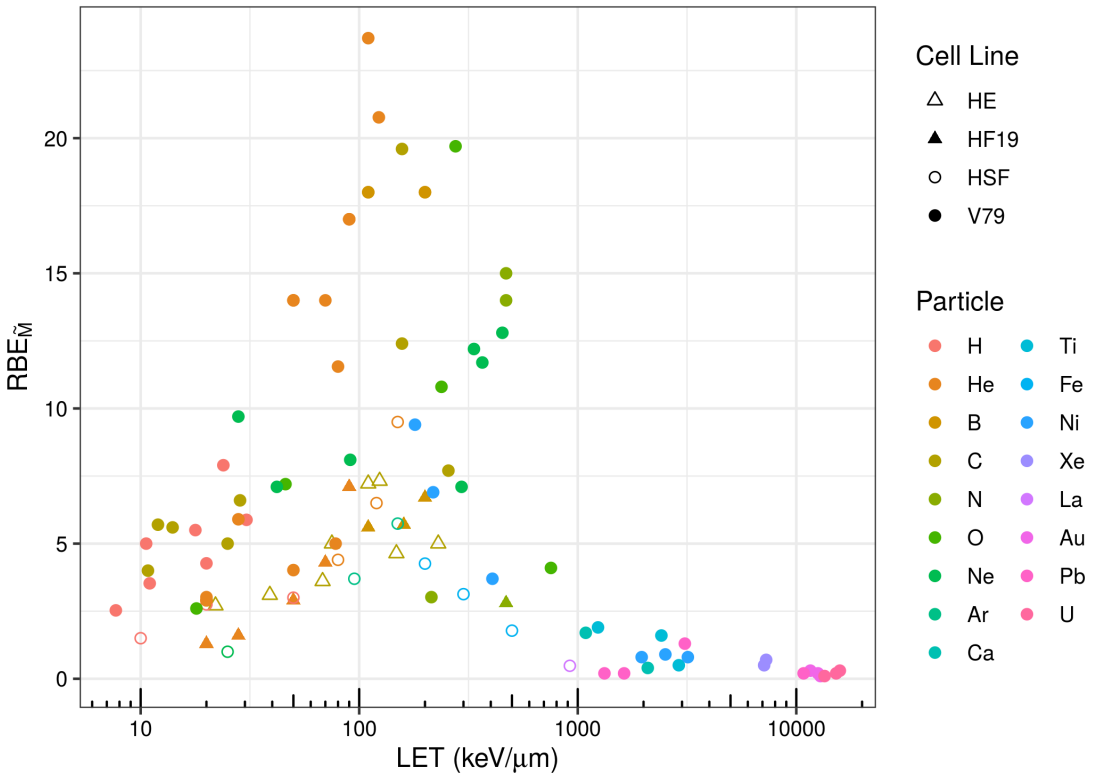

Figure 3: Scatter plot showing the RBE for mutation induction as retrieved from previous publications. All available data are presented together, different cell lines and particle species are identified with a combination of symbol and colour as shown in the Figure legend.

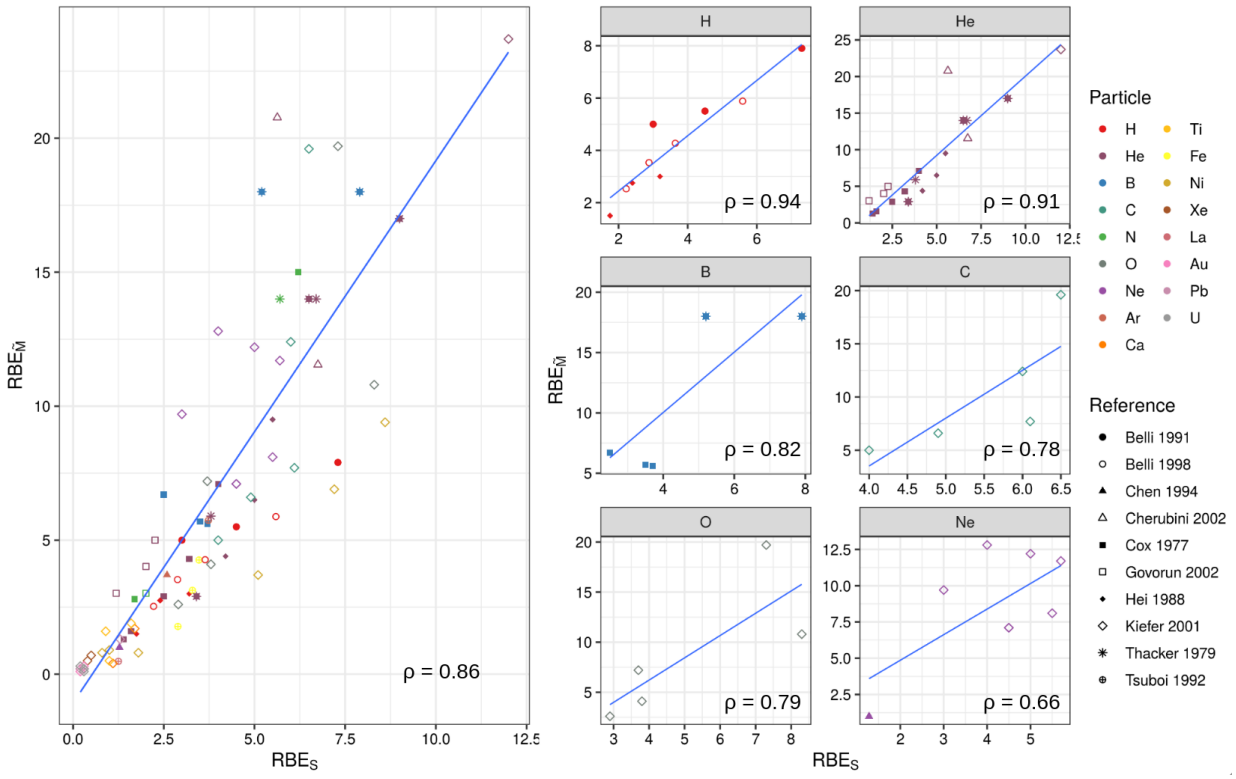

Figure 4: Correlation analysis between $RBE_{\tilde{M}}$ and RBE_S literature data. Global view (left), detailed analysis resolved for different particle species (right). When available from different publications, data relative to the same particle species are pooled together and identified as shown in the legend. The Pearson correlation coefficient was calculated and is shown in each panel. Such correlation coefficient was significant ($p<0.05$) for H, He and B and for the pooled data.

We are now going to present the results of the modelling analysis applied to the different available data sets. Figure 5 shows the data obtained when considering the data set from Belli et al, consisting in V79 cells irradiated with protons up to 30.5 keV/µm. In order to better appreciate the trends, modelling calculations were performed on an extended LET range up to 80 keV/µm. MKM evaluations look in good agreement with experimental data. This is obtained by adopting a reduced domain size for mutation induction compared to survival (see Table 2). On the right plot we can appreciate the increasing

difference between overall induced and observable mutations, with the latter approaching saturation at the highest LET. A similar trend is observed when analysing the data obtained with helium and boron irradiation by Cox and Thacker (Figure 6). Here, the model well describes the helium data for both survival and mutation induction, while larger deviations are observed for boron data. Specifically, the model overestimates RBE_S at the lowest LET, while showing the tendency toward an underestimation of $RBE_{\tilde{M}}$, despite still being inside experimental error bars. However, it must be noticed that experimental data are available only for two LET values. Again, a lower domain size allows achieving a good agreement between observed and predicted mutations. Finally, the results of He, C and O irradiation were considered by analysing the data by Kiefer et al (Figure 7; no error bars were available in the publication). One single experimental data point was available for Helium, which limits the robustness of the analysis. In this case, the model seems to underestimate survival after He irradiation, while the agreement improves for mutation induction. When considering C and O data, the typical trend of RBE curves is observed both for survival and mutation induction, with RBE increasing with LET before decreasing at the highest LET values. A reasonable agreement is observed here, with the largest deviations reported for C ion, with RBE_S being somewhat underestimated at low LET. The model appears to nicely reproduce oxygen data, even though the limits of track-segment condition are approached at the highest LETs. Figure 8 reports the χ^2 analyses on which the choice of the domain size for mutation induction is based. The domain size corresponding to the minimum χ^2 is indicated by a triangle, while different colours indicate the different datasets. The Figure shows that the

agreement with experimental data improves by reducing the domain size, until a point when a further reduction results in a χ^2 increases.

Table 2. Values of the parameters used in the MC-MKM evaluations for the three datasets (Belli *et al* 1998, Cox *et al* 1977, Thacker *et al* 1979) and (Kiefer *et al* 2001).

		Survival parameters				**Mutation parameters**			
Data Set	**Particle**	**α_x (Gy^{-1})**	**β_x (Gy^{-2})**	**R_N (µm)**	**R_d (µm)**	**α'_x (Gy^{-1})**	**β'_x (Gy^{-2})**	**$R'_N=R_N$ (µm)**	**R'_d (µm)**
Belli 1998	H	0.129	0.046	3.96	0.34	6.03×10^{-6}	1.2×10^{-6}	3.96	0.23
Cox 1977, Thacker 1979	He, B	0.143	0.026	3.45	0.29	2.93×10^{-6}	9.72×10^{-7}	3.45	0.24
Kiefer 2001	He, C, O	0.241	0.076	4.54	0.34	1.61×10^{-6}	1.33×10^{-6}	4.54	0.29

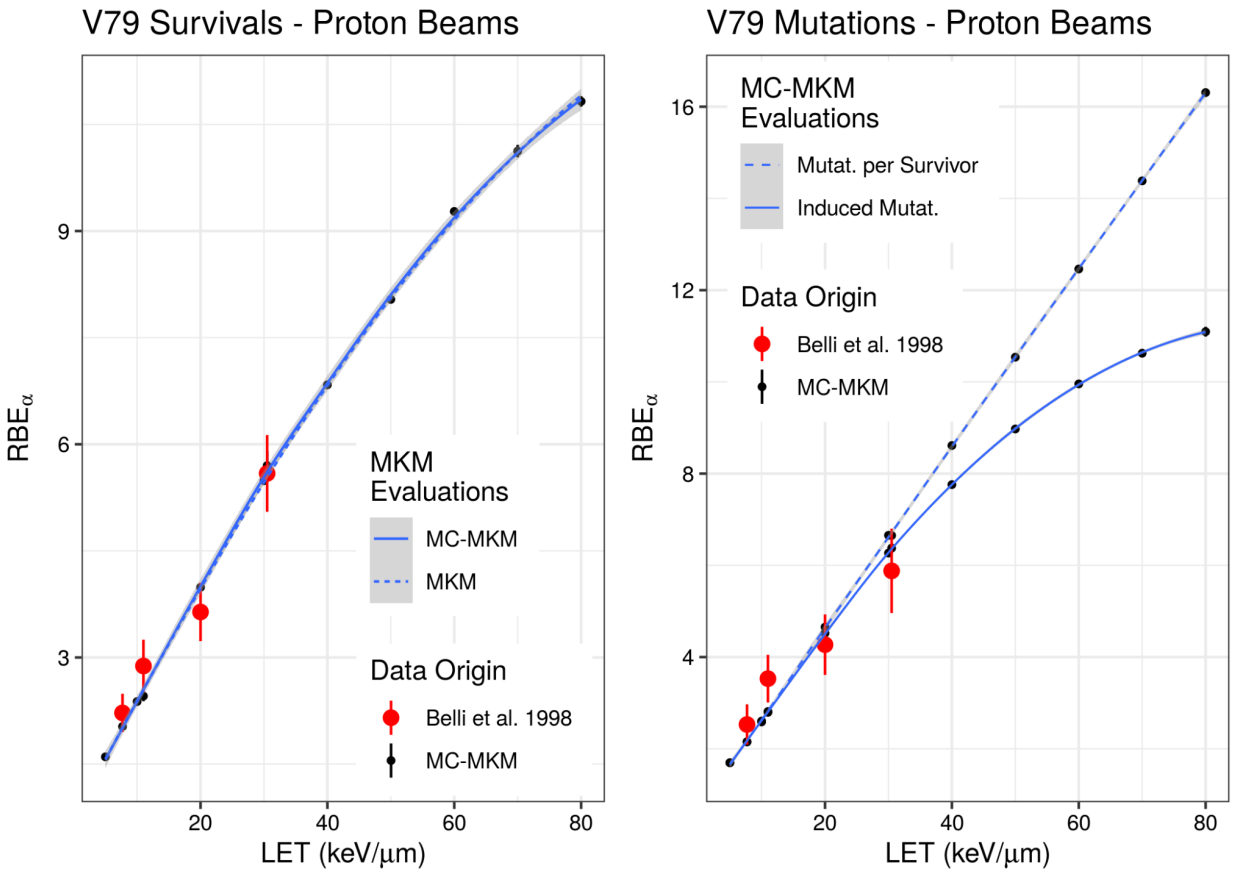

Figure 5: Results of the modelling analysis applied to the proton irradiation data published in (Belli *et al* 1998). Experimental RBE for survival (left panel) and mutation (right panel) are shown by red symbols (observed mutation per survivor), while the black dots are MKM evaluations performed with the MC-MKM evaluation method (Manganaro *et al* 2017) for both overall induced mutations and mutations per survivor. Blue lines are interpolations of the discrete model evaluations performed with a LOESS algorithm. In the case of survival RBE, model evaluations are performed using both the MC-MKM and the analytical MKM implementation described in (Kase *et al* 2008).

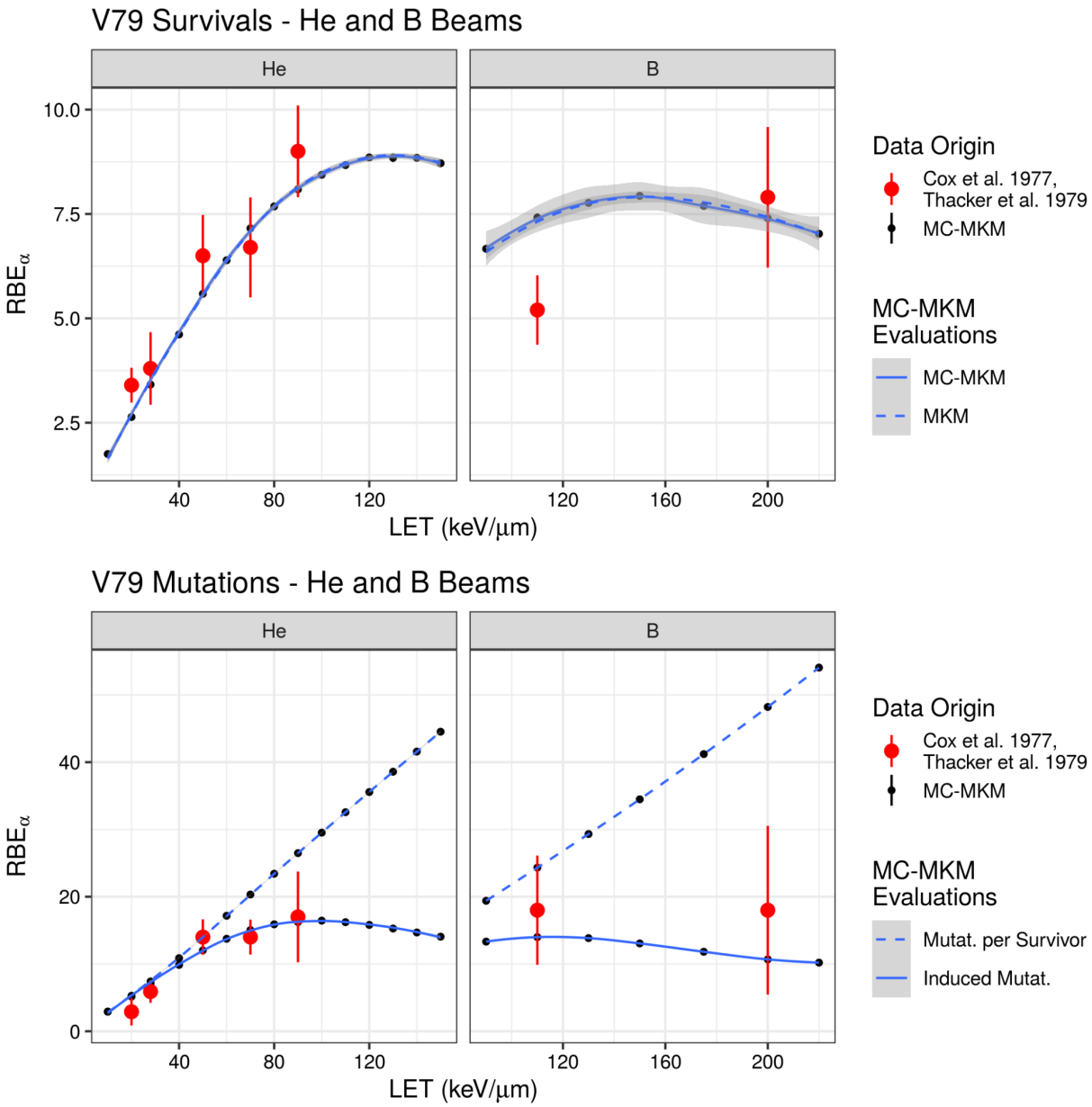

Figure 6: Results of the modelling analysis applied to the He and B irradiation data published in (Cox *et al* 1977) and in (Thacker *et al* 1979). Experimental RBE for survival (upper panels) and mutation (bottom panels) are shown by red symbols (observed mutation per survivor), while the black dots are MKM evaluations performed with the MC-MKM evaluation method (Manganaro *et al* 2017) for both overall induced mutations and mutations per survivor. Blue lines are interpolations of the discrete model evaluations performed with a LOESS algorithm. In the case of survival RBE, model evaluations are performed using both the MC-MKM and the analytical MKM implementation described in (Kase *et al* 2008).

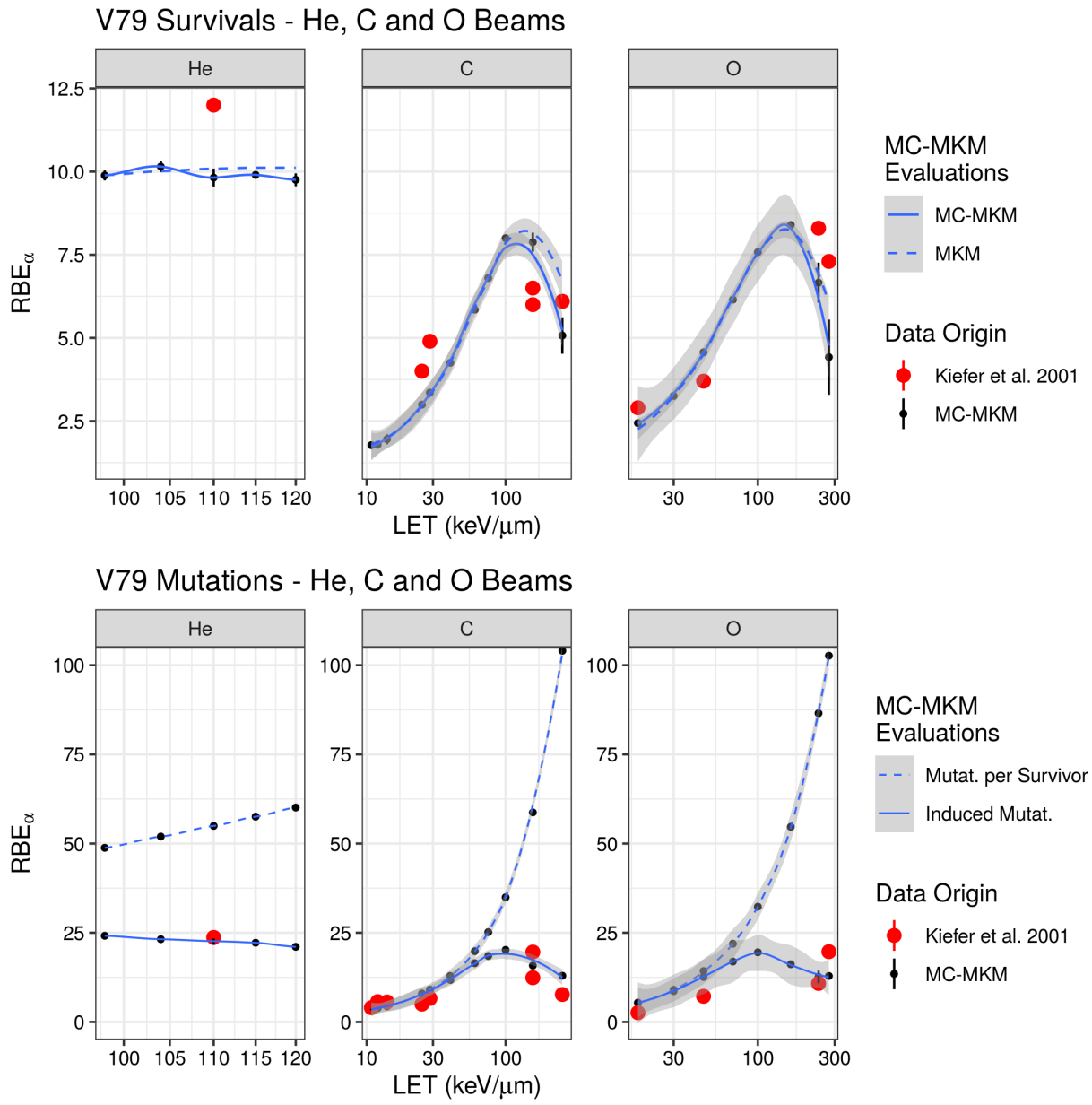

Figure 7: Results of the modelling analysis applied to the He, C and O irradiation data published in (Kiefer *et al* 2001). Experimental RBE for survival and observed mutation per survivor are shown by red symbols, while the black dots are MKM evaluations performed with the MC-MKM evaluation method (Manganaro *et al* 2017). Experimental uncertainties are not reported in the original paper. Blue lines are interpolations of the discrete model evaluations performed with a LOESS algorithm. In the case of survival RBE, model evaluations are performed using both the MC-MKM and the analytical MKM implementation described in (Kase *et al* 2008).

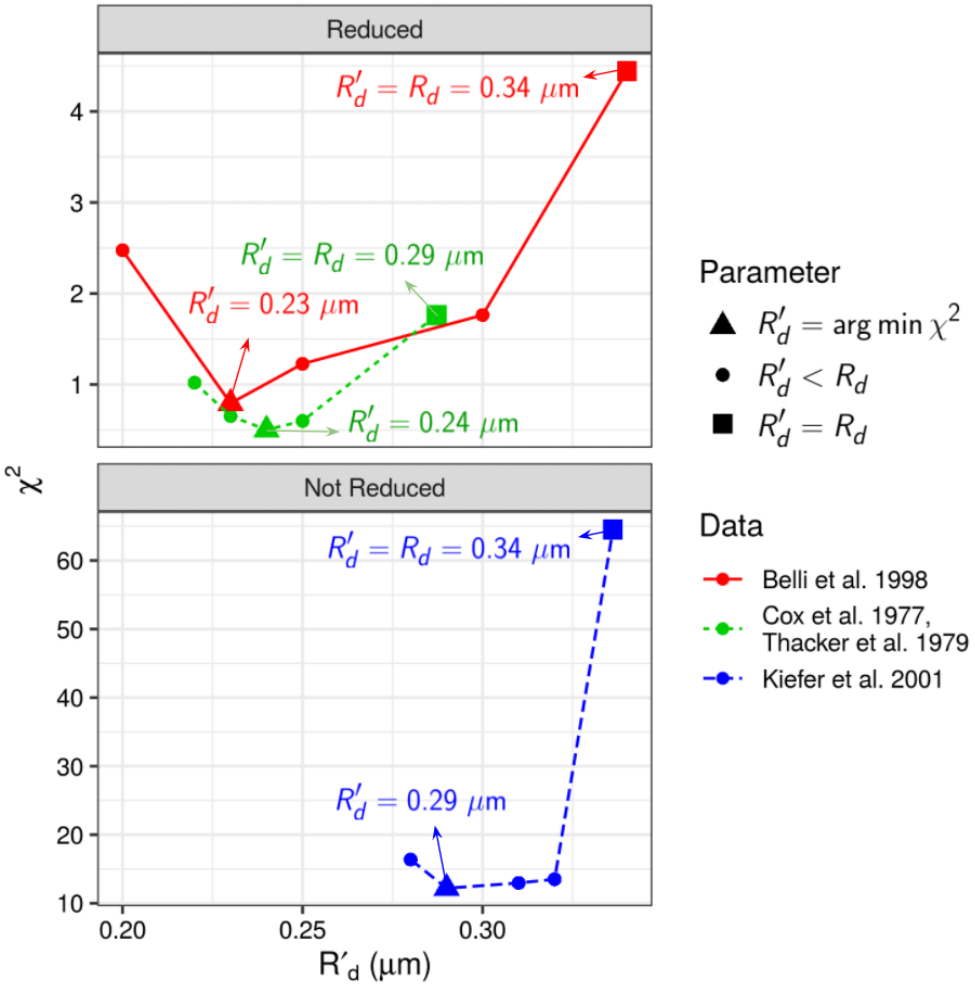

Figure 8: χ^2 as a function of the parameter R'$_d$ (domain radius for the mutations), for the datasets from (Belli *et al* 1998, Cox *et al* 1977, Thacker *et al* 1979) and (Kiefer *et al* 2001). The values corresponding to $R'_d = R_d$ (square) and to the minimum of χ^2 (triangle) are annotated in the plot. The lower plot shows not reduced χ^2 values because of the lack of experimental errors (Kiefer *et al* 2001).

Discussion

This study investigated the possibility to establish an MKM based modelling framework for the combined analysis of cell survival and mutation induction following exposure to particle irradiation. To this purpose, a database was set-up collecting from literature a large set of RBE data based on the *hprt* mutation assay. Despite the efforts performed to retrieve the largest amount of data, we cannot exclude that few publications were not

included in the current version of the database, which will be eventually integrated in the future. The database, which is available online (https://doi.org/10.5281/zenodo.6451956), contains overall 115 entries and triggers some considerations on the availability of experimental data for this specific endpoint. Firstly, the amount of data is remarkably small compared to what is available in terms of survival RBE (see for instance (Friedrich *et al* 2013)). Moreover, all data were obtained before 2003 (no later data were found in literature) and are relative to monoenergetic irradiation. To our knowledge, no modulated field measurements have been performed with this assay. The lack of more recent data can be partially attributed to drawbacks of the experimental method, being the *hprt* assay a time and resource consuming approach. At the same time, survival RBE has been considered of primary importance for a long time, being the potential for tumour eradication the first requisite for the establishment of CPT.

Growing interest has been registered in recent years toward radiotherapy-induced toxicity, including late effects such as secondary cancer induction. In this context, special attention is deserved for instance by paediatric, lymphoma and breast cancer patients treated with protons, according to the comparably good survival and long-life expectancy (Cella *et al* 2013, Abo-Madyan *et al* 2014, Paganetti *et al* 2020, Cartechini *et al* 2020). This is also relevant for particle beams heavier than protons, whose use is prospectively increasing. While several modelling approaches are available for the estimation of SCR following radiotherapy, such models generally neglect the possibility to consider a variable RBE for protons (and heavier particles). Recently, the publication by Hufnagl et al. tried to partially fill this gap, by extending the LEM formalism to the analysis of

mutation-related endpoints (i.e. *in vitro* cell transformations, *in vivo* carcinogenesis in mice Harderian glands). The present study is complementary to the latter, being based both on a different modelling formalism (i.e. MKM instead of LEM) as well as on a different specific endpoint (i.e. mutation induction vs cell transformation), less directly related to cancer induction, but where a larger and more systematic amount of experimental data is available. Furthermore, the Monte Carlo implementation used in the present modelling approach, i.e. the MC-MKM, is able to reproduce more accurately the correlated statistics between survival and mutation induction without the analytical approximations needed in the other approach (Manganaro *et al* 2017). However, in principle, our formalism could be applied to the transformation data as well. While we explored with the MKM the major alternative formalism to LEM, typically applied to RBE_S calculation, including in clinical applications, the specific different features and parameters of the two approaches assume clearly a different role and interpretation in the present application to mutation/transformation induction. In fact, while the two models share some common parameters, namely the photon LQ response ones, α_x and β_x, and the cellular nucleus size R_N, LEM considers the threshold dose D_t for transition from a LQ behaviour to a purely linear one in the reference radiation response, where MKM, instead, includes as a parameter a domain size R_d. Indeed, in Hufnagl, a second value for D_t (i.e. $D_{t(T)}$) is responsible for the specific transformation probability, while in our case a different domain size value is taken R'_d. This difference, besides being purely connected to a parameter choice, defines a different interpretation of the conceptual relation between the 2 distinct processes of cell killing and transformation. In the present case, the

specific choice allows a closer connection to possible mechanistic pathways. In fact, an interesting result of the modelling analysis is indeed that one related to the domain size. Our results indicate that overall a reduced domain size for mutation induction compared to that used for the survival analysis allows maximizing the agreement between predicted $RBE_{\tilde{M}}$ and experimental data. Remarkably, this reduced domain size is consistently found in the analysis of three independent data sets. On the one hand, this could point toward different biological sub-structures being associated with the two endpoints. On the other hand, reducing the domain structure translates into a modification of the microdosimetric spectrum that produces the observed effect (see Figure 1). More in general, these results could point toward the use of a fixed domain size as one of the main limitations of the standard MKM framework. Efforts are currently being made in our group to propose a "domain-free" modified MKM framework on the basis of an alternative, recently developed, stochastic model (Cordoni *et al* 2021).

One limitation of this study is related to the intrinsic characteristics of the experimental method. The *hprt* mutation assay provides information on the mutation rate induced by irradiation of a specific gene. Such mutation rate could be different for other genes, according to their size, their localization etc. On top of that, it is known that radiation carcinogenesis is a multi-step process and *in vitro* mutation experiments can capture only part of this complex process, providing indications that are mainly related to the so-called initiation step. From this point of view, the results obtained with our approach should not be regarded as indicative of the absolute SCR following exposure to different radiation qualities, but rather of the relative differences that could be expected after photon and

charged particle irradiation concerning mutation induction risks. That's why the use of an RBE for such process is more robust.

Further developments of the present work are on going and include the application of the $RBE_{\tilde{M}}$ to the estimation of SCR after proton therapy plans. In this context, SCR models proposed in the past and recently tested also by our group will be expanded (Schneider 2009, Schneider and Walsh 2008, Cartechini *et al* 2020), taking into account the impact of a variable RBE for both cell survival and mutation induction. According to the current discussion on the clinical use of a variable RBE in proton therapy, this will contribute to shed light on the risks of side effects related to this technique and thus also to improve the patient selection procedure.

Conclusions

We reported on a novel framework for modelling mutation induction from different particle beams based on an extension of the MKM. From a systematic collection of 105 data from 12 publications, it emerges a strong correlation between RBE_S and $RBE_{\tilde{M}}$, especially for lighter particles such as p, He and B, with an overall correlation factor $\rho=0.86$, ($p<0.005$). MKM modelling has been adapted to the description of mutation induction, thus presenting a first successful translation of the MKM to the analysis of mutation-related endpoints. Remarkably, a smaller domain size is needed for the description of mutation compared to survival data. This modelling framework, because of the close analogy with the RBE_S modelling can be readily implemented in

treatment planning and applied for the predictions of SCR in therapeutic as well as in space mission radioprotection scenarios.

References

Abo-Madyan Y, Aziz M H, Aly M M O M, Schneider F, Sperk E, Clausen S, Giordano F A, Herskind C, Steil V, Wenz F and Glatting G 2014 Second cancer risk after 3D-CRT, IMRT and VMAT for breast cancer *Radiother. Oncol.* **110** 471–6 Online: https://linkinghub.elsevier.com/retrieve/pii/S0167814013006439

Balcer-Kubiczek E K and Eley J G 2018 Secondary Malignancies in the Era of High-Precision Radiation Therapy *Crit. Rev. Oncog.* **23** 93–112 Online: http://www.dl.begellhouse.com/journals/439f422d0783386a,15fcae2c28ac4859,2b6a767f41db8d0a.html

Belli M, Cera F, Cherubini R and Dall M 1998 RBE-LET relationships for cell inactivation and mutation induced by low energy protons in V79 cells: further results at the LNL facility *Int. J. Radiat. Biol.* **74** 501–9 Online: http://www.tandfonline.com/doi/full/10.1080/095530098141375

Cartechini G, Fracchiolla F, Menegotti L, Scifoni E, La Tessa C, Schwarz M, Farace P and Tommasino F 2020 Proton pencil beam scanning reduces secondary cancer risk in breast cancer patients with internal mammary chain involvement compared to photon radiotherapy *Radiat. Oncol.* **15** 228 Online: https://ro-journal.biomedcentral.com/articles/10.1186/s13014-020-01671-8

Cella L, Conson M, Pressello M C, Molinelli S, Schneider U, Donato V, Orecchia R, Salvatore M and Pacelli R 2013 Hodgkin's lymphoma emerging radiation treatment techniques: trade-offs between late radio-induced toxicities and secondary malignant neoplasms. *Radiat. Oncol.* **8** 22 Online: http://www.pubmedcentral.nih.gov/articlerender.fcgi?artid=3641014&tool=pmcentrez&rendertype=abstract

Chen D J, Tsuboi K, Nguyen T and Yang T C 1994 Charged-particle mutagenesis II. Mutagenic effects of high energy charged particles in normal human fibroblasts. *Adv. Space Res.* **14** 347–54 Online: http://www.ncbi.nlm.nih.gov/pubmed/11539970

Cherubini R, Canova S, Favaretto S, Bruna V, Battivelli P and Celotti L 2002 Minisatellite and Hprt mutations in V79 cells irradiated with helium ions and gamma rays *Int. J. Radiat. Biol.* **78** 791–7 Online: http://www.tandfonline.com/doi/full/10.1080/09553000210146572

Cordoni F, Missiaggia M, Attili A, Welford S M, Scifoni E and La Tessa C 2021 Generalized stochastic microdosimetric model: The main formulation *Phys. Rev. E* **103** 012412 Online: https://link.aps.org/doi/10.1103/PhysRevE.103.012412

Cox R, Masson W K, Thacker J, Stretch A and Stephens M A 1979 Mutation and inactivation of cultured mammalian cells exposed to beams of accelerated heavy ions. II. Chinese hamster V79 cells. *Int. J. Radiat. Biol. Relat. Stud. Phys. Chem. Med.* **36** 149–60 Online: http://www.ncbi.nlm.nih.gov/pubmed/315388

Cox R, THACKER J, GOODHEAD D T and MUNSON R J 1977 Mutation and inactivation of mammalian cells by various ionising radiations *Nature* **267** 425–7

Online: http://www.nature.com/articles/267425a0

Durante M, Debus J and Loeffler J S 2021 Physics and biomedical challenges of cancer therapy with accelerated heavy ions *Nat. Rev. Phys.* Online: https://www.nature.com/articles/s42254-021-00368-5

Durante M and Flanz J 2019 Charged particle beams to cure cancer: Strengths and challenges *Semin. Oncol.* **46** 219–25 Online: https://linkinghub.elsevier.com/retrieve/pii/S0093775419300788

Ebner D K, Frank S J, Inaniwa T, Yamada S and Shirai T 2021 The Emerging Potential of Multi-Ion Radiotherapy *Front. Oncol.* **11** Online: https://www.frontiersin.org/articles/10.3389/fonc.2021.624786/full

Friedrich T, Scholz U, Elsässer T, Durante M and Scholz M 2012 Calculation of the biological effects of ion beams based on the microscopic spatial damage distribution pattern *Int. J. Radiat. Biol.* **88** 103–7

Friedrich T, Scholz U, Elsässer T, Durante M and Scholz M 2013 Systematic analysis of RBE and related quantities using a database of cell survival experiments with ion beam irradiation *J. Radiat. Res.* **54** 494–514

Hawkins R B 1996 A microdosimetric-kinetic model of cell death from exposure to ionizing radiation of any LET, with experimental and clinical applications *Int. J. Radiat. Biol.* **69** 739–55 Online: http://www.tandfonline.com/doi/full/10.1080/095530096145481

Hawkins R B 1998 A microdosimetric-kinetic theory of the dependence of the RBE for cell death on LET *Med. Phys.* **25** 1157–70 Online:

http://doi.wiley.com/10.1118/1.598307

Hei T K, Chen D J, Brenner D J and Hall E J 1988 Mutation induction by charged particles of defined linear energy transfer *Carcinogenesis* **9** 1233–6 Online: https://academic.oup.com/carcin/article-lookup/doi/10.1093/carcin/9.7.1233

Hufnagl A, Scholz M and Friedrich T 2021 Modeling Radiation-Induced Neoplastic Cell Transformation In Vitro and Tumor Induction In Vivo with the Local Effect Model *Radiat. Res.* **195** Online: https://bioone.org/journals/radiation-research/volume-195/issue-5/RADE-20-00160.1/Modeling-Radiation-Induced-Neoplastic-Cell-Transformation-In-Vitro-and-Tumor/10.1667/RADE-20-00160.1.full

Inaniwa T and Kanematsu N 2018 Adaptation of stochastic microdosimetric kinetic model for charged-particle therapy treatment planning *Phys. Med. Biol.* **63** 095011 Online: https://iopscience.iop.org/article/10.1088/1361-6560/aabede

Inaniwa T, Suzuki M, Furukawa T, Kase Y, Kanematsu N, Shirai T and Hawkins R B 2013 Effects of Dose-Delivery Time Structure on Biological Effectiveness for Therapeutic Carbon-Ion Beams Evaluated with Microdosimetric Kinetic Model *Radiat. Res.* **180** 44–59 Online: http://www.bioone.org/doi/10.1667/RR3178.1

Johnson G E 2012 Mammalian Cell HPRT Gene Mutation Assay: Test Methods pp 55–67 Online: http://link.springer.com/10.1007/978-1-61779-421-6_4

Kase Y, Kanai T, Matsufuji N, Furusawa Y, Elsässer T and Scholz M 2008 Biophysical calculation of cell survival probabilities using amorphous track structure models for heavy-ion irradiation *Phys. Med. Biol.* **53** 37–59 Online: https://iopscience.iop.org/article/10.1088/0031-9155/53/1/003

Kellerer A M and Rossi H H 1978 A Generalized Formulation of Dual Radiation Action *Radiat. Res.* **75** 471 Online: https://www.jstor.org/stable/3574835?origin=crossref

Kiefer J, Schmidt P and Koch S 2001 Mutations in mammalian cells induced by heavy charged particles: an indicator for risk assessment in space. *Radiat. Res.* **156** 607–11 Online: http://www.ncbi.nlm.nih.gov/pubmed/11604081

Kiefer J, Schreiber A, Gutermuth F, Koch S and Schmidt P 1999 Mutation induction by different types of radiation at the Hprt locus *Mutat. Res. Mol. Mech. Mutagen.* **431** 429–48 Online: https://linkinghub.elsevier.com/retrieve/pii/S0027510799001840

Krämer M, Scifoni E, Schuy C, Rovituso M, Tinganelli W, Maier A, Kaderka R, Kraft-Weyrather W, Brons S, Tessonnier T, Parodi K and Durante M 2016 Helium ions for radiotherapy? Physical and biological verifications of a novel treatment modality *Med. Phys.* **43** 1995–2004 Online: http://doi.wiley.com/10.1118/1.4944593

Kranert T, Schneider E and Kiefer J 1990 Mutation induction in V79 Chinese hamster cells by very heavy ions. *Int. J. Radiat. Biol.* **58** 975–87

Manganaro L, Russo G, Cirio R, Dalmasso F, Giordanengo S, Monaco V, Muraro S, Sacchi R, Vignati A and Attili A 2017 A Monte Carlo approach to the microdosimetric kinetic model to account for dose rate time structure effects in ion beam therapy with application in treatment planning simulations. *Med. Phys.* **44** 1577–89 Online: http://www.ncbi.nlm.nih.gov/pubmed/28130821

Mohamad O, Makishima H and Kamada T 2018 Evolution of Carbon Ion Radiotherapy at the National Institute of Radiological Sciences in Japan *Cancers (Basel).* **10** 66 Online: https://www.mdpi.com/2072-6694/10/3/66

Paganetti H 2012 Assessment of the Risk for Developing a Second Malignancy From Scattered and Secondary Radiation In Radiation Therapy *Health Phys.* **103** 652–61 Online: https://journals.lww.com/00004032-201211000-00019

Paganetti H, Depauw N, Johnson A, Forman R B, Lau J and Jimenez R 2020 The risk for developing a secondary cancer after breast radiation therapy: Comparison of photon and proton techniques *Radiother. Oncol.* **149** 212–8 Online: https://linkinghub.elsevier.com/retrieve/pii/S0167814020302917

Rackwitz T and Debus J 2019 Clinical applications of proton and carbon ion therapy *Semin. Oncol.* **46** 226–32 Online: https://linkinghub.elsevier.com/retrieve/pii/S0093775419300570

Schneider U 2009 Mechanistic model of radiation-induced cancer after fractionated radiotherapy using the linear-quadratic formula *Med. Phys.* **36** 1138–43 Online: http://doi.wiley.com/10.1118/1.3089792

Schneider U and Walsh L 2008 Cancer risk estimates from the combined Japanese A-bomb and Hodgkin cohorts for doses relevant to radiotherapy *Radiat. Environ. Biophys.* **47** 253–63 Online: http://link.springer.com/10.1007/s00411-007-0151-y

Scholz M, Kellerer A M, Kraft-Weyrather W and Kraft G 1997 Computation of cell survival in heavy ion beams for therapy: The model and its approximation *Radiat. Environ. Biophys.* **36** 59–66

Sokol O, Scifoni E, Tinganelli W, Kraft-Weyrather W, Wiedemann J, Maier A, Boscolo D, Friedrich T, Brons S, Durante M and Krämer M 2017 Oxygen beams for therapy: advanced biological treatment planning and experimental verification *Phys. Med.*

Biol. **62** 7798–813 Online: https://iopscience.iop.org/article/10.1088/1361-6560/aa88a0

Stoll U, Barth B, Scheerer N, Schneider E and Kiefer J 1996 HPRT mutations in V79 Chinese hamster cells induced by accelerated Ni, Au and Pb ions. *Int. J. Radiat. Biol.* **70** 15–22

Stoll U, Schmidt A, Schneider E and Kiefer J 1995 Killing and mutation of Chinese hamster V79 cells exposed to accelerated oxygen and neon ions. *Radiat. Res.* **142** 288–94

Suzuki M, Watanabe M, Kanai T, Kase Y, Yatagai F, Kato T and Matsubara S 1996 LET dependence of cell death, mutation induction and chromatin damage in human cells irradiated with accelerated carbon ions. *Adv. Space Res.* **18** 127–36 Online: http://www.ncbi.nlm.nih.gov/pubmed/11538953

Thacker J, Stretch A and Stephens M A 1979 Mutation and Inactivation of Cultured Mammalian Cells Exposed to Beams of Accelerated Heavy Ions *Int. J. Radiat. Biol. Relat. Stud. Physics, Chem. Med.* **36** 137–48 Online: http://www.tandfonline.com/doi/full/10.1080/09553007914550891

Tommasino F, Scifoni E and Durante M 2015 New Ions for Therapy *Int. J. Part. Ther.* **2** 428–38 Online: http://theijpt.org/doi/10.14338/IJPT-15-00027.1

Tsuboi K, Yang T C and Chen D J 1992 Charged-particle mutagenesis. 1. Cytotoxic and mutagenic effects of high-LET charged iron particles on human skin fibroblasts. *Radiat. Res.* **129** 171–6 Online: http://www.ncbi.nlm.nih.gov/pubmed/1734447